Journal of Alloys and Compounds 509 (2011) 5562–5566

Contents lists available at ScienceDirect

Journal of Alloys and Compounds

journal homepage: www.elsevier.com/locate/jallcom

Influence of the addition of vanadium on the hydrogenation properties of the compounds $TiFe_{0.9}V_x$ and $TiFe_{0.8}Mn_{0.1}V_x$ ($x = 0$, 0.05 and 0.1)

A. Guéguen, M. Latroche*

Institut de Chimie et des Matériaux de Paris Est (ICMPE), Chimie Métallurgique des Terres Rares, CNRS, UMR 7182, 2-8 rue Henri Dunant, 94320 Thiais, France

ARTICLE INFO

Article history:
Received 26 December 2010
Received in revised form 3 February 2011
Accepted 4 February 2011
Available online 21 March 2011

Keywords:
TiFe
Hydrogen storage materials
EPMA
Pressure hysteresis

ABSTRACT

$TiFe_{0.9}$ and $TiFe_{0.8}Mn_{0.1}$ hydrides have suitable equilibrium pressures at ambient conditions and are potential candidates for hydrogen storage applications. In this work, we study the influence of the addition of small amounts of vanadium on the hydrogenation properties of $TiFe_{0.9}V_x$ and $TiFe_{0.8}Mn_{0.1}V_x$ ($x = 0$, 0.05 and 0.1) alloys. The excess of Ti from TiFe in these materials results in the precipitation of Ti and Ti_2Fe-type phases. In the analysis of the chemical composition, vanadium was observed in small amount in all phases for each sample which contains vanadium. Vanadium tends to substitute Fe sites, which results in a decrease of the plateau pressures. The addition of vanadium as $TiFe_{0.8}Mn_{0.1}V_x$ ($x = 0.05$ and 0.1) alloys has beneficial effects on the equilibrium plateaus of the hydrides: the plateaus become flatter and a significant reduction in the pressure hysteresis is observed.

1. Introduction

Among the different AB compounds (with A a transition metal or a rare earth element and B a transition metal) considered for hydrogen storage, FeTi (CsCl structure type) was found to exhibit the highest gravimetric absorption capacity (1.9 wt% at 40 °C) and suitable plateau pressures [1]. However, the binary alloy is not suitable for hydrogen storage because of the difficulty to activate the material and its slow kinetics. Several studies were carried out to understand the reasons of such difficult activation. A summary of the results was published by Schlapbach and Riesterer [2]. During activation, the TiFe lattice expands and contracts about 20% of its volume. As a result, the surface/volume ratio increases significantly. FeTi is then very reactive, not only towards hydrogen but also oxygen, resulting in the formation of an oxide layer which acts as a barrier for hydrogen diffusion [3]. Problems of activation attributed to slow diffusion of hydrogen in the bulk material were also observed in ultrapure TiFe [2]. The activation issue can be overcome by adding a small excess of Ti to TiFe [4–6]. The formation of β-Ti hydride occurs before the hydrogenation of the TiFe phase, resulting in the creation of cracks making easier the diffusion of hydrogen through the bulk.

Challet et al. studied the partial substitution of Fe by Mn in $TiFe_{0.9}$ [7]. The alloy $TiFe_{0.8}Mn_{0.1}$ can absorb up to 1.92 wt% at 25 °C. The sample could be activated at room temperature without any thermal treatment and 90% of the maximum capacity was absorbed within 157 s. The Pressure–Composition–Isotherm (PCI) curves of $TiFe_{0.8}Mn_{0.1}$ present two absorption plateaus and two desorption plateaus. However, the equilibrium pressures of the compound $TiFe_{0.8}Mn_{0.1}$ are still low at 25 °C (0.122 and 0.244 MPa for absorption and 0.065 and 0.188 MPa for desorption). For hydrogen storage in portable devices, materials with equilibrium desorption pressures about 0.1–1 MPa at room temperature are required.

Massicot recently studied the hydrogenation properties of a compound TiFe containing 5 at.% V (nominal composition $Ti_{47}V_5Fe_{48}$) [8]. Like TiFe, the activation of the sample required severe thermal treatment. The kinetics were quite slow as well. Interestingly a single pressure plateau was observed for $Ti_{47}V_5Fe_{48}$ at 25 °C on the PCI curves whereas two plateaus were reported by Reilly for TiFe [9]. Detailed X-ray studies of the hydrogenation process of TiFe indicated the existence of two orthorhombic hydrides β_1 and β_2 (FeTiH and $TiFeH_{1.4}$) and a hydrogen rich monoclinic phase γ [10]. A single pressure plateau was also observed by Mitrokhin et al. who studied the hydrogenation properties of TiFe-type Ti–Fe–Mn–V alloys [11,12]. In these alloys, vanadium substitutes for iron and titanium and the decomposition pressure of the β- and γ-hydride approaches each other. As a result, the two corresponding plateaus transform into one sloping plateau. They called this phenomenon the "pressure smoothing effect". Metallic vanadium atom has a larger radius than that of iron. As a result, the equilibrium pressures for $Ti_{47}V_5Fe_{48}$ were lower than those of TiFe. Two suitable characteristics for hydrogen storage were observed in the case of $Ti_{47}V_5Fe_{48}$: little hysteresis between absorption and desorption and smooth equilibrium plateaus.

In order to understand this result, the effects of the addition of small amounts of vanadium to $TiFe_{0.9}$ and $TiFe_{0.8}Mn_{0.1}$ on the hydrogenation properties of $TiFe_{0.9}V_x$ and $TiFe_{0.8}Mn_{0.1}V_x$ ($x = 0$,

* Corresponding author. Tel.: +33 1 49 78 12 10; fax: +33 1 49 78 12 03.
E-mail addresses: michel.latroche@icmpe.cnrs.fr, latroche@glvt-cnrs.fr (M. Latroche).

0925-8388/$ – see front matter © 2011 Elsevier B.V. All rights reserved.
doi:10.1016/j.jallcom.2011.02.036

Table 1
Nominal composition of the $TiFe_{0.9}V_x$ ($x = 0$, 0.05, 0.1) alloys, structure, chemical composition and relative amount of the different phases present in the materials.

Sample no.	Nominal composition	Phase	Structure type	Fraction	Composition	Cell parameters (Å)
1	$TiFe_{0.9}$	Matrix	CsCl	94.8 (9)	$Ti_{51.4(3)}Fe_{48.6(3)}$	$a = 2.98187$ (7)
		Ti-type precipitates	$P6_3/mmc$	2.12 (2)	$Ti_{80.1(4)}Fe_{19.7(4)}$	$a = 2.964$ (2) $c = 4.621$ (4)
		Ti_2Fe-type precipitates	Fd-3m	3.06 (2)	$Ti_{66.8(4)}Fe_{33.2(4)}$	$a = 11.321$ (6)
2	$TiFe_{0.9}V_{0.05}$	Matrix	CsCl	95.9 (9)	$Ti_{50.4(4)}Fe_{47.3(5)}V_{2.2(2)}$	$a = 2.9867$ (3)
		Ti-type precipitates	$P6_3/mmc$	3.3 (3)	$Ti_{70.3(4)}Fe_{21.9(5)}V_{7.8(2)}$	$a = 2.929$ (2) $c = 4.580$ (5)
		Ti_2Fe-type precipitates	Fd-3m	0.84 (1)	$Ti_{61.4(6)}Fe_{33.0(6)}V_{5.6(3)}$	$a = 11.296$ (14)
3	$TiFe_{0.9}V_{0.1}$	Matrix	CsCl	94.6 (9)	$Ti_{48.4(5)}Fe_{47.7(9)}V_{3.9(5)}$	$a = 2.9891$ (2)
		Ti-type precipitates	$P6_3/mmc$	3.7 (2)	$Ti_{62.6(4)}Fe_{23.3(8)}V_{14.1(5)}$	$a = 2.898$ (1) $c = 4.597$ (4)
		Ti_2Fe-type precipitates	Fd-3m	1.6 (3)	$Ti_{58.2(3)}Fe_{32.9(5)}V_{8.9(3)}$	$a = 11.290$ (9)

Table 2
Nominal composition of the $TiFe_{0.8}Mn_{0.1}V_x$ ($x = 0$, 0.05, 0.1) compounds, structure, chemical composition and relative amount of the different phases present in the materials.

Sample no.	Nominal composition	Phase	Structure type	Fraction	Composition	Cell parameters (Å)
4	$TiFe_{0.8}Mn_{0.1}$	Matrix	CsCl	97.0 (9)	$Ti_{52.0(2)}Fe_{43.1(5)}Mn_{4.8(4)}$	$a = 2.9888$ (2)
		Ti-type precipitates	$P6_3/mmc$	1.7 (2)	$Ti_{77.3(7)}Fe_{18.1(7)}Mn_{4.56\ (6)}$	$a = 2.955$ (2) $c = 4.624$ (5)
		Ti_2Fe-type precipitates	Fd-3m	1.3 (2)	$Ti_{66.4(4)}Fe_{29.7(4)}Mn_{3.94(5)}$	$a = 11.326$ (6)
5	$TiFe_{0.8}Mn_{0.1}V_{0.05}$	Matrix	CsCl	97.0 (10)	$Ti_{50.6(1)}Fe_{41.7(6)}Mn_{4.7(3)}V_{3.0(1)}$	$a = 2.9940$ (2)
		Ti-type precipitates	$P6_3/mmc$	2.4 (2)	$Ti_{69.0(1)}Fe_{17.70(5)}Mn_{4.56(2)}V_{8.75(3)}$	$a = 2.932$ (2) $c = 4.590$ (4)
		Ti_2Fe-type precipitates	Fd-3m	0.68 (7)	$Ti_{60.3(3)}Fe_{29.2(4)}Mn_{4.1(2)}V_{6.3(3)}$	$a = 11.325$ (5)
6	$TiFe_{0.8}Mn_{0.1}V_{0.1}$	Matrix	CsCl	96.2 (9)	$Ti_{49.4(4)}Fe_{41.3(7)}Mn_{4.7(3)}V_{4.6(2)}$	$a = 2.9959$ (2)
		Ti-type precipitates	$P6_3/mmc$	3.4 (2)	$Ti_{63.8(5)}Fe_{18.9(6)}Mn_{4.73(7)}V_{12.6(3)}$	$a = 2.887$ (1) $c = 4.696$ (3)
		Ti_2Fe-type precipitates	Fd-3m	0.46 (8)	$Ti_{57.9(11)}Fe_{28.8(23)}Mn_{4.6(4)}V_{8.7(11)}$	$a = 11.305$ (8)

0.05 and 0.1) alloys were studied. The structure and composition of the resulting alloys were investigated using powder X-ray diffraction and Electron Probe Microanalysis Analysis (EPMA). The hydrogenation properties (activation, kinetics, thermodynamics) are also described and compared to vanadium free compounds.

2. Experimental details

All samples were synthesized by melting high purity elements (Ti 99.99% from Alfa Aesar, V 99.9% from ChemPur, Fe 99.98% from Sigma–Aldrich and Mn 99.99% from ChemPur) in an induction furnace with a water-cooled copper hearth under argon atmosphere. The ingots were melted five times and turned over each time to ensure a good homogeneity. After fusion, the ingots were wrapped in a tantalum foil, annealed in silica tubes at 1000 °C for 1 week under Ar atmosphere and quenched in water to remove any concentration gradient created during induction melting.

Powder X-ray diffraction (PXRD) data were collected at room temperature on a Bruker D8 Advance (Cu Kα, Bragg Brentano geometry, 2θ range 20–100°, step size 0.02°). All the patterns were refined with the Rietveld method using the program FullProf [13].

The chemical analysis was performed on finely polished samples using an EPMA Cameca SX 100. Segregation of minor phases in the bcc matrix was studied using Backscattered Electron (BSE) microscopy. Accelerating voltage and beam current were 15 kV and 40 mA, respectively. The composition of each phase in the alloys was determined from 10 to 100 measurement points at the surface of the polished samples.

The Pressure–Composition–Isotherm (PCI) curves were measured with a Sieverts type apparatus. All manipulations before exposure to pure hydrogen gas (99.9999% from Alphagaz) were carried out under argon. Activations were performed at 25 °C under 2.5 MPa of hydrogen. All samples could be activated under these conditions. Dehydrogenation of the samples was carried out by applying primary vacuum at 25 °C for 2 h.

3. Results and discussion

3.1. Structural characterizations

Six samples (1–6) with nominal composition $TiFe_{0.9}V_x$ and $TiFe_{0.8}Mn_{0.1}V_x$ ($x = 0$, 0.05 and 0.1) were synthesized, the composition of which are chosen by adding 0%, 5% and 10% V to $TiFe_{0.9}$ and $TiFe_{0.8}Mn_{0.1}$. They consist mainly of a TiFe phase in which Ti and Ti_2Fe-type phases are also observed (Tables 1 and 2).

The PXRD patterns for compounds 1, 2 and 3 are shown in Fig. 1. The most intense peaks belong to the TiFe cubic phase. However, minor peaks of low intensity in the region 39–42° are observed for all compounds. The extra peaks could be indexed as Ti- and Ti_2Fe-type structure. The presence of these secondary phases is consistent with the results reported by Challet et al. [7] who observed such precipitates in $TiFe_{0.8}Mn_{0.1}$. The precipitation of such phases is caused by the excess of Ti used. Rietveld refinement on the PXRD data of compounds 1, 2 and 3 indicated a low content of these secondary phases (<4 wt%). Similar PXRD patterns were obtained for compounds 4, 5 and 6 (Fig. 2) which consisted of a main CsCl-type phase and small amounts of Ti and Ti_2Fe phases.

For all our samples, the cell parameters of the major phase increase with the amount of vanadium. This is an indication that

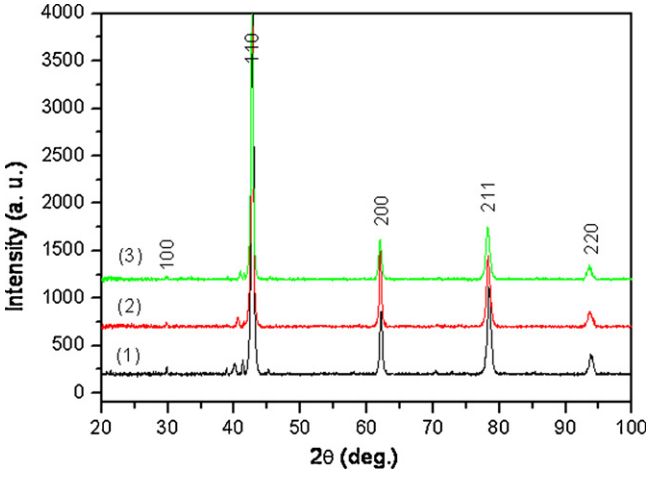

Fig. 1. Powder X-ray diffraction patterns of alloys 1, 2 and 3 with nominal composition $TiFe_{0.9}V_x$ ($x = 0$, 0.05 and 0.1). Minor peaks of low intensity are observed in the region 39–42° besides the main TiFe-type phase. *hkl* indexes stand for the main phase (TiFe).

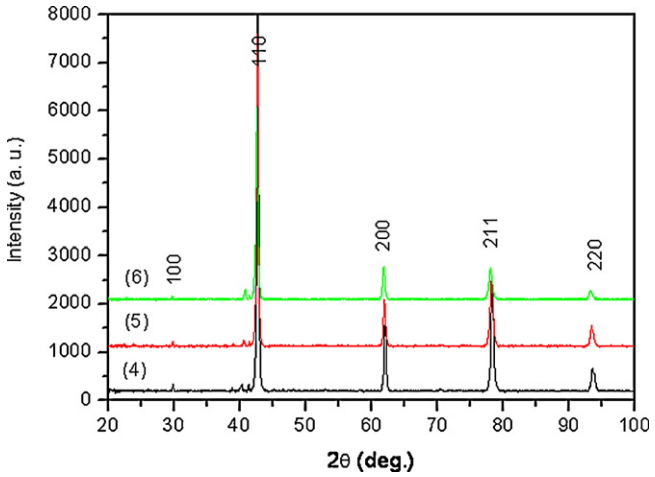

Fig. 2. Powder X-ray diffraction patterns of alloys 4, 5 and 6 with nominal composition $TiFe_{0.8}Mn_{0.1}V_x$ (x = 0, 0.05 and 0.1). Minor peaks are observed in the area 39–42°.

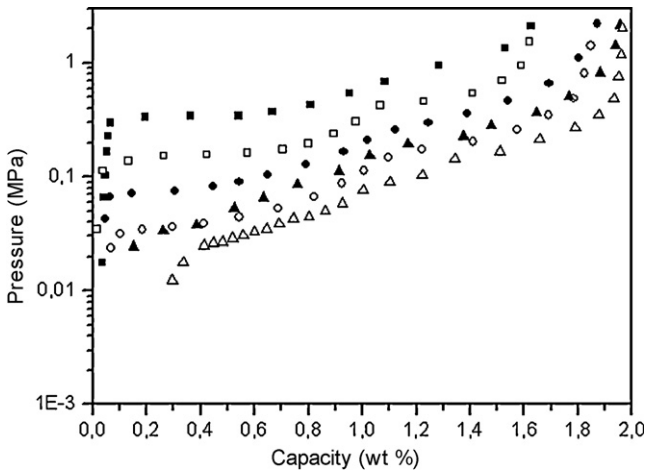

Fig. 4. PCI curves at 25 °C for the alloys 1 (■), 2 (●) and 3 (▲). Absorption data correspond to plain symbols, desorption data to empty ones.

vanadium tends to substitute Fe in the B sites. By comparing the experimental and calculated density measured for $TiFe_{0.7}Mn_{0.1}$, Challet showed that the excess of Ti was on the Fe site [7]. However, in this study, by Rietveld refinement putting vanadium in Ti or Fe sites did not influence the result. This could be attributed to the fact that the applied amount of vanadium is relatively small.

The chemical composition of the different phases present in the samples was determined using EPMA analysis. By BSE microscopy on finely polished samples, precipitations were observed. Two examples of images obtained for compounds 2 and 6 are shown in Fig. 3. EPMA results for the six alloys are summarized in Tables 1 and 2.

The amounts of Ti and Fe in the $TiFe_{0.9}V_x$ compounds (x = 0, 0.05 and 0.1) are similar, a small quantity of V is also present in the composition of the matrix in the case of $TiFe_{0.9}V_{0.05}$ and $TiFe_{0.9}V_{0.1}$. For these compounds, Ti-type phase contains iron and a little vanadium. Vanadium was also found in the Ti_2Fe-type precipitates. These results are consistent with the Fe–Ti–V phase diagram reported by Massicot et al. [14]. The alloys 1, 2 and 3 lie outside of the limit of the TiFe single phase domain. The composition $Ti_{47}V_5Fe_{48}$ studied by Massicot [8] is inside the TiFe domain and secondary phase was not observed.

The same observations about the $TiFe_{0.8}Mn_{0.1}V_x$ samples were done. Vanadium is present in small quantities in the matrix of $TiFe_{0.8}Mn_{0.1}V_{0.05}$ and $TiFe_{0.8}Mn_{0.1}V_{0.1}$. Vanadium is also found in the two types of precipitates. These results are consistent with the information obtained by PXRD.

3.2. Hydrogenation properties

3.2.1. $TiFe_{0.9}V_x$ (x = 0, 0.05 and 0.1) alloys

All samples could be activated without any thermal treatment. The presence of Ti- and Ti_2Fe-type precipitates in the TiFe matrix seems to play a significant role in the initiation of hydrogen absorption in our materials. Our three compositions, all containing Ti and Ti_2Fe-type precipitates, could be easily activated whereas for TiFe and $Ti_{47}V_5Fe_{48}$ severe thermal treatment was required to initiate the hydrogenation [1,8]. This is in good agreement with previous results reported by Matsumoto [15]. He observed, using *in situ* X-ray diffraction, that, in TiFe-based alloys containing β-Ti phase, the β-Ti phase hydrogenated before the TiFe matrix, thus creating cracks. These cracks help the diffusion of hydrogen through the bulk and create new reactive surface. After five activation cycles, the absorption kinetics of $TiFe_{0.9}V_x$ (x = 0, 0.05 and 0.1) alloys were studied. 90% of the maximal absorption capacity was reached after 72, 59 and 55 s for $TiFe_{0.9}$, $TiFe_{0.9}V_{0.05}$ and $TiFe_{0.9}V_{0.1}$, respectively. The absorption kinetics of vanadium containing samples was improved.

The PCI curves of the $TiFe_{0.9}V_x$ (x = 0.05 and 0.1) compounds were collected at 25 °C during absorption and desorption (Fig. 4). The maximal absorption capacity increases as a function of vanadium content: $TiFe_{0.9}$ absorbs 1.63 wt% of hydrogen and $TiFe_{0.9}V_{0.1}$

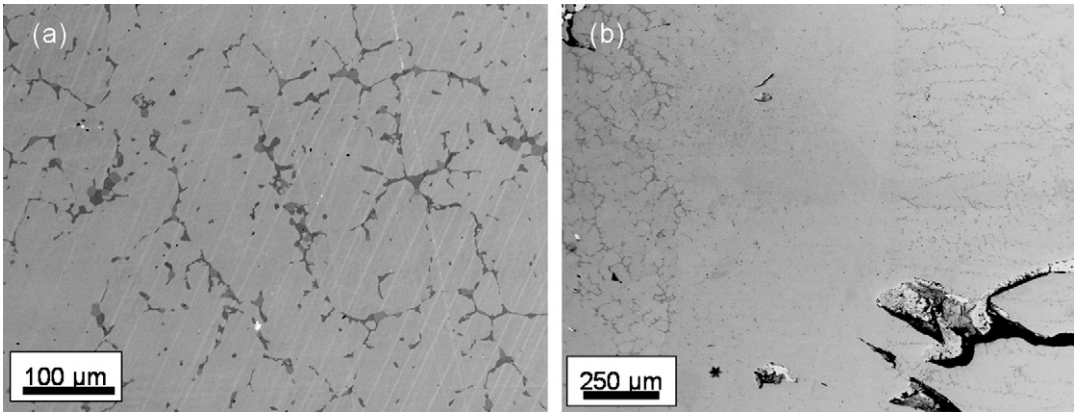

Fig. 3. BSE images of (a) compound 2 and (b) compound 6. Two different types of precipitates are observed in the TiFe matrix. Brighter areas are Ti-type phases and darker ones Ti_2Fe-type phases.

Table 3
Hydrogenation properties of the $TiFe_{0.9}V_x$ (x = 0, 0.05, 0.1) compounds at 25 °C: maximal and reversible capacities, equilibrium pressures during absorption and desorption.

Sample no.	Nominal composition	Maximal capacity (wt%)	Reversible capacity (wt%)	t_{90}[a] (s)	Equilibrium pressure for absorption (MPa)			Equilibrium pressure for desorption (MPa)		
					1st Plateau	2nd Plateau	$\ln(P_2/P_1)$	1st Plateau	2nd Plateau	$\ln(P_2/P_1)$
1	$TiFe_{0.9}$	1.62	1.56	72	0.337	0.998	1.086	0.160	0.471	1.080
2	$TiFe_{0.9}V_{0.05}$	1.88	1.60	59	0.076	0.312	1.412	0.037	0.188	1.626
3	$TiFe_{0.9}V_{0.1}$	1.96	1.74	55	0.036	0.232	1.863	0.039	0.145	1.313

NB: the reversible capacity was estimated by taking the beginning of the first desorption plateau and the end of the second plateau as limits.
[a] t_{90} is defined as the time needed to absorb 90% of the maximal capacity.

Table 4
Hydrogenation properties of the $TiFe_{0.8}Mn_{0.1}V_x$ (x = 0, 0.05, 0.1) compounds at 25 °C: maximal and reversible capacities, equilibrium pressures during absorption and desorption.

Sample no.	Nominal composition	Maximal capacity (wt%)	Reversible capacity (wt%)	t_{90}[a] (s)	Equilibrium pressure for absorption (MPa)			Equilibrium pressure for désorption (MPa)		
					1st Plateau	2nd Plateau	$\ln(P_2/P_1)$	1st Plateau	2nd Plateau	$\ln(P_2/P_1)$
4	$TiFe_{0.8}Mn_{0.1}$	1.68	1.60	50	0.109	0.190	0.556	0.059	0.142	0.878
5	$TiFe_{0.8}Mn_{0.1}V_{0.05}$	1.71	1.58	41	0.034	0.109	1.165	0.022	0.076	1.240
6	$TiFe_{0.8}Mn_{0.1}V_{0.1}$	1.76	1.52	19	0.017	0.081	1.561	0.013	0.063	1.578

NB: the reversible capacity was estimated by taking the beginning of the first desorption plateau and the end of the second plateau as limits.
[a] t_{90} is defined as the time needed to absorb 90% of the maximal capacity.

1.96 wt%. As the affinity of vanadium for hydrogen is higher than that of iron, partial substitution of iron by vanadium results in an increase in the absorption capacity.

All PCI curves present two equilibrium plateaus. The equilibrium pressures decrease with the amount of V. This is in good agreement with the increase in the cell parameters of the TiFe phase observed by PXRD. The capacity of the first plateau was reduced and the slope of the second plateau increased with the amount of vanadium. For x = 0.1, it is hard to determine precisely the equilibrium pressure of the second plateau. During desorption, the difference between the equilibrium plateaus decreases with the amount of V, this agrees with the "pressure smoothing effect" described by Mitrokhin in TiFe-type Ti–Fe–Mn–V [12] (see Table 3).

3.2.2. $TiFe_{0.8}Mn_{0.1}V_x$ (x = 0, 0.05 and 0.1) alloys

All samples could be activated without any thermal treatment. This could be attributed to the influence of the Ti and Ti_2Fe-type precipitates on the activation of the hydrogen absorption of the TiFe alloys as all the samples contain Ti and Ti_2Fe-type precipitates. No significant difference in the kinetics is observed when comparing the three alloys: 90% of the maximal absorption capacity is reached within less than 1 min (Table 4).

The total absorption capacity increases slightly with the amount of vanadium. The increase of hydrogen storage capacity is not as significant as that observed for the $TiFe_{0.9}V_x$ samples. This is probably due to the presence of Mn and V in the Fe sites. The affinity of Mn for hydrogen is not as strong as that of V. As a result, the absorption capacity of $TiFe_{0.8}Mn_{0.1}$ is not increased too much when adding V.

The PCI curves of the $TiFe_{0.8}Mn_{0.1}V_x$ (x = 0, 0.05 and 0.1) compounds were collected at 25 °C during absorption and desorption (Fig. 5). All present two equilibrium plateaus. Significant differences on the PCI curves are visible. First, the equilibrium pressures decrease with the amount of vanadium. This is consistent with the increase of the cell parameters of the matrix observed from PXRD data. Then, for each composition, the pressure difference between the two plateaus increases with the amount of vanadium. The value of $\ln(P_2/P_1)$ (P_1 and P_2 being the 1st and 2nd equilibrium pressures) varies between 0.556 for $TiFe_{0.8}Mn_{0.1}$ and 1.561 for $TiFe_{0.8}Mn_{0.1}V_{0.1}$ during hydrogen absorption and 0.878 and 1.578 during the desorption process. This suggests that vanadium modifies the relative stability of the hydrides, the β hydride becoming more stable.

Another interesting feature is the decrease in hysteresis with the addition of vanadium. Very little hysteresis is observed for $TiFe_{0.8}Mn_{0.1}V_{0.1}$. Pressure hysteresis is an undesirable phenomenon as it represents a loss in energy and efficiency. Thus the addition of vanadium to $TiFe_{0.8}Mn_{0.1}$ has a beneficial effect on the pressure hysteresis of the alloy. Several studies about the effects of partial substitution of metal on the pressure hysteresis in AB_2 and AB_5 alloys have been reported [16,17]. Partial substitution of Mn by V in $Ti_{0.95}Zr_{0.05}Cr_{1.2}Mn_{0.8}$ resulted also in a reduction of the pressure hsyteresis [16]. Reduced hysteresis was also observed in Ce-based AB_5 where the nickel metal is partially replaced by Al, Sn or Co [17]. Several theories to understand the hysteresis phenomenon have been proposed [18–22]. A review of all these studies was issued by Qian [23]. According to most theoretical models, the main reason for such decrease in pressure hysteresis is the strain of the crystalline matrix induced during hydride formation and decomposition. The strain is caused by the lattice volume expansion as the α phase transforms into the β phase. In this study, such reduction in pressure hysteresis is not observed for the $TiFe_{0.9}V_x$ (x = 0, 0.05 and 0.1) alloys, this implies that Mn also plays a significant role in the hydrogenation process. Moreover, flatter plateaus

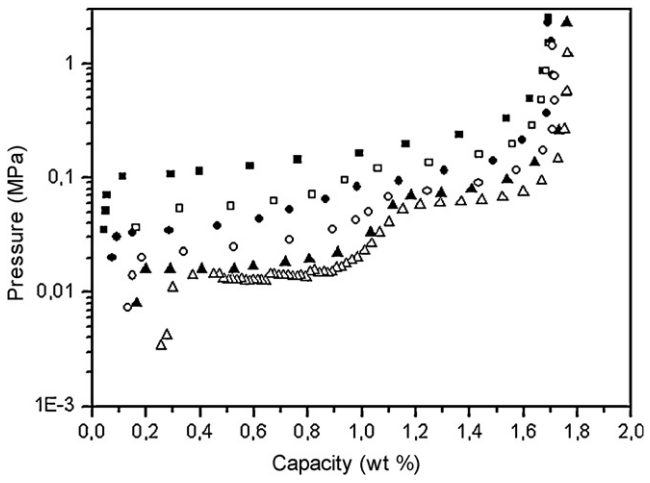

Fig. 5. PCI curves at 25 °C for the alloys 4 (■), 5 (●) and 6 (▲). Absorption data correspond to plain symbols, desorption data to empty ones.

are obtained for the $TiFe_{0.8}Mn_{0.1}V_x$ compounds. A detailed analysis by PXRD of the structural defects generated during the α to β transformation would be worth to be done.

4. Conclusion

$TiFe_{0.9}V_x$ and $TiFe_{0.8}Mn_{0.1}V_x$ ($x = 0$, 0.05 and 0.1) alloys have been synthesized using induction melting. In order to ensure a good homogeneity, the ingots were annealed 1 week at 1000 °C. All samples consist of a main TiFe phase in which Ti and Ti_2Fe-type precipitates are observed. Vanadium was confirmed in both the matrix and the precipitates. All compounds absorb hydrogen without any thermal treatment because of the presence of Ti-type precipitates. The lattice constant of the matrix decreases with the amount of vanadium, which results in a decrease of the plateau pressures. Smaller hydrogen capacity and more tilted pressure plateaus were observed for $TiFe_{0.9}V_{0.05}$ and $TiFe_{0.9}V_{0.1}$ when compared to $TiFe_{0.9}$. The main advantage of the addition of V to $TiFe_{0.9}$ is an increase in the absorption capacity. The addition of vanadium to $TiFe_{0.8}Mn_{0.1}$ has several beneficial effects for hydrogen storage: the pressure hysteresis decreases with the vanadium content and the pressure plateaus are flatter.

Acknowledgment

The authors would like to thank Dr. E. Leroy for all EPMA analyzes and the ANR agency through the Pan-H program for funding.

References

[1] J. Reilly, R. Wiswall, Inorg. Chem. (1974) 218.
[2] L. Schlapbach, T. Riesterer, Appl. Phys. A 32 (1983) 169.
[3] J.J. Reilly, F. Reidinger, J. Less-Common Met. 85 (1982) 145.
[4] T. Mizuno, T. Morozumi, J. Less-Common Met. 84 (1982) 237.
[5] S.M. Lee, T.P. Perng, J. Less-Common Met. 177 (1991) 107.
[6] X. Wang, R. Chen, C. Chen, Q. Wang, J. Alloys Compd. 425 (2006) 291.
[7] S. Challet, M. Latroche, F. Heurtaux, Proceedings of the "Materials for the Hydrogen Economy" Symposium: Materials Science and Technology, 2005, p. 13.
[8] B. Massicot, Study of the Fe–Ti–V System and its Application for Hydrogen Storage, Université Paris XII, France, 2009, http://tel.archives-ouvertes.fr/docs/00/44/29/63/PDF/These_Massicot.pdf.
[9] J.J. Reilly, J.R. Johnson, in: IAHE (Ed.), Proceedings of the 1st World Hydrogen Energy Conference, 1976, p. 8B.
[10] F. Reidinger, J. Lynch, J. Reilly, J. Phys. F 12 (1982) L49.
[11] S.V. Mitrokhin, V.N. Verbetsky, K.N. Semenenko, Zh. Obshch. Khim. 61 (1991) 785.
[12] S.V. Mitrokhin, V.N. Verbetsky, R.R. Kajumov, H. Cunmao, Z. Yufen, J. Alloys Compd. 199 (1993) 155.
[13] J. Rodríguez-Carvajal, in: XV Congress of Int. Union of Crystallography, Satellite Meeting on Powder Diffraction, Toulouse, France, 1990, p. 127.
[14] B. Massicot, J.M. Joubert, M. Latroche, Int. J. Mater. Res. 11 (2010) 1413.
[15] T. Matsumoto, M. Amano, Y. Sasaki, J. Less-Common Met. 88 (1982) 443.
[16] M.T. Hagström, S.N. Klyamkin, P.D. Lund, J. Alloys Compd. 293–295 (1999) 67.
[17] S.N. Klyamkin, M.T. Hagström, E.V. Mescheryakova, P.D. Lund, J. Mater. Sci. 35 (2000) 133.
[18] A.R. Ubbelohde, Proc. R. Soc. London, Ser. A 159 (1937) 295.
[19] J.R. Lacher, Proc. R. Soc. London, Ser. A 161 (1937) 525.
[20] D.H. Everett, P. Nordon, Proc. R. Soc. London, Ser. A (1960) 341.
[21] N.A. Schultus, W.K. Hall, J. Chem. Phys. 39 (1963) 868.
[22] T.B. Flanagan, J.D. Clewley, J. Less-Common Met. 83 (1982) 127.
[23] S. Qian, D.O. Northwood, Int. J. Hydrogen Energy 13 (1988) 25.